Enhanced Photonic Band-Gap Confinement via Van Hove Saddle Point Singularities

Mihai Ibanescu, Evan J. Reed,* and J. D. Joannopoulos

Department of Physics, Massachusetts Institute of Technology, Cambridge, Massachusetts 01239, USA

(Received 18 February 2005; published 26 January 2006)

We show that a saddle point Van Hove singularity in a band adjacent to a photonic crystal band gap can lead to situations which defy the conventional wisdom that the strongest band-gap confinement is found at frequencies near the midgap. As an example, we present a two-dimensional square photonic crystal waveguide where the strongest confinement is close to the *band edge*. The underlying mechanism can also apply to any system that is described by a band structure with a gap. In general, the saddle point favors the appearance of a very flat band, which in turn results in an enhanced confinement at band-gap frequencies immediately above or below the flat band.

DOI: 10.1103/PhysRevLett.96.033904 PACS numbers: 42.70.Qs, 41.20.Jb, 42.82.Et

Confinement of light by photonic band gaps is at the base of a majority of photonic crystal devices and applications [1–6]. For the simplest photonic crystal, a one-dimensional Bragg grating, the strongest light confinement is found near the midgap frequency, and this intuitive result is often extended to higher-dimensional photonic crystal structures as well. However, in a recent Letter [7], Li *et al.* have reported numerical results showing a surprising frequency dependence of the band-gap localization of a mode in a two-dimensional (2D) photonic crystal waveguide. The strongest localization was found not at the midgap frequency, but at frequencies much closer to the upper edge of the complete band gap. Here, we discover the origin of this effect as a consequence of the presence of a saddle point Van Hove singularity in the dispersion relation of the photonic band immediately above the gap. Periodicity-induced band gaps are also central to electronic, magnonic, and phononic band structures in solid state physics [8–10]. Because the enhanced confinement effect presented here is an intrinsic property of the bulk band structure of a crystal, it should be encountered in these systems as well.

To illustrate our results we use the example photonic crystal waveguide structure recently analyzed by Li *et al.* As shown in Fig. 1(a), a waveguide is created by removing a row of rods from a square lattice of dielectric rods in air. The lattice period is a and the rods have radius $0.18a$ and index of refraction 3.4. For the transverse magnetic polarization (magnetic field in the plane), the photonic crystal possesses a complete photonic band gap in the angular frequency range $0.302–0.443$ $(2\pi c/a)$. Band-gap confinement results in a guided mode of the waveguide, whose field profile is shown schematically as a red line and whose dispersion relation is plotted as a black line in Fig. 1(b). If the surrounding photonic crystal cladding has only a finite number of layers some of the power in the waveguide mode will radiate outside and the mode becomes leaky [7,11]. During numerical experiments on this waveguide mode, Li *et al.* observed a surprising frequency dependence of the loss coefficient. Instead of finding the lowest loss at a frequency close to the midgap frequency, they found that the radiation loss keeps decreasing as the frequency is increased almost to the upper limit of the complete photonic band gap. They also confirmed that this lower loss is consistent with a more tightly localized mode.

To understand the localization of the waveguide mode in the transverse (y) direction, we investigate the properties of the evanescent bulk modes that make up the cladding tails of the waveguide mode. For a given frequency ω and longitudinal Bloch wave vector k_x, let $\{k_y^{(n)}\}$ be the infinite set of solutions for the transverse wave vector k_y of the bulk photonic crystal modes, with n being an integer index. (In vacuum, with the same boundary conditions, the solutions would be given by $k_y^{(n)} = [(\omega/c)^2 - (k_x + 2n\pi/a)^2]^{1/2}$ with n taking integer values). Band-gap confinement exists only at (ω, k_x) pairs for which all k_y solutions have a nonzero imaginary part and are therefore evanescent in the y direction. For values of y far from the core of the waveguide the slowest-decaying mode dominates, which means that the strength of the band-gap confinement is best described by the smallest imaginary part of k_y over all solutions [12]. Thus, we define the confinement strength to be $\kappa(\omega, k_x) = \min_n(|\mathrm{Im}[k_y^{(n)}(\omega, k_x)]|)$.

The complex-valued transverse wave vectors $k_y^{(n)}$ of the bulk crystal modes are calculated via a frequency-domain eigenmode-expansion method implemented in the freely available CAMFR code [13]. We present the resulting confinement strength κ as a color contour plot in Fig. 1(b). The black regions correspond to no confinement since propagating states exist in the bulk crystal for those (ω, k_x) pairs. Red and yellow regions represent increasingly stronger confinement, as shown in the colorbar. Figure 1(c) displays the strong asymmetry of the confinement strength $\kappa(\omega, k_x(\omega))$ along the dispersion relation $k_x(\omega)$ of the guided mode. Instead of finding the strongest confinement at a frequency near the midgap, we see that κ increases throughout most of the complete band gap up to a frequency of $0.425(2\pi c/a)$, very close to the upper edge of the gap.

The key to this surprising behavior of the band-gap confinement can be found by looking at the bulk photonic crystal band structure which is shown in blue in Fig. 2. The

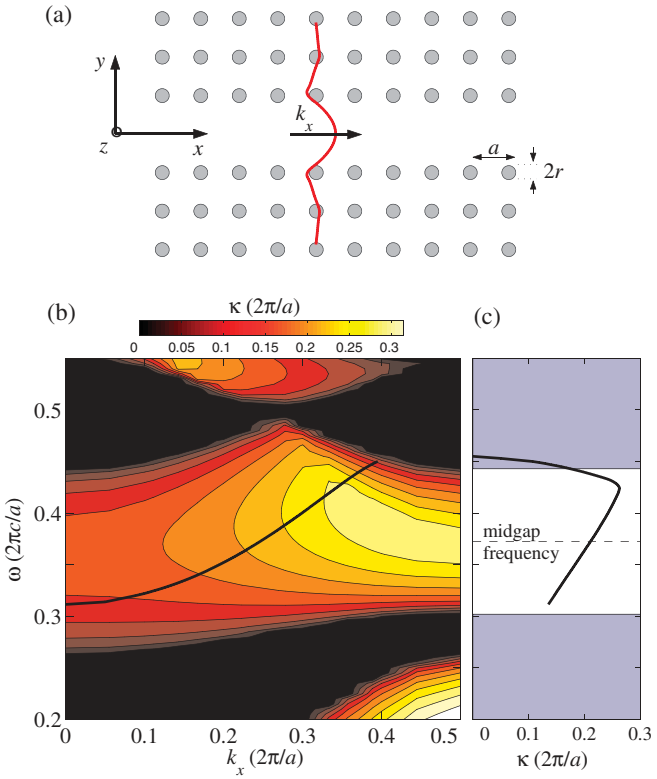

FIG. 1 (color). (a) A waveguide is formed by removing one row from a 2D square lattice of dielectric rods with refractive index 3.4 and radius $r = 0.18a$. (b) The dispersion relation of the waveguide mode (thick black line) is shown on top of a color contour plot of the confinement strength of the bulk photonic crystal $\kappa(\omega, k_x)$. The black regions include (ω, k_x) pairs for which propagating modes exist in the bulk crystal, while the colors from dark red to bright yellow represent increasingly stronger confinement, as shown by the colorbar. (c) Confinement strength κ along the dispersion relation of the guided mode. The gray areas delimit the complete band-gap range. The y axis is the same as in part (b).

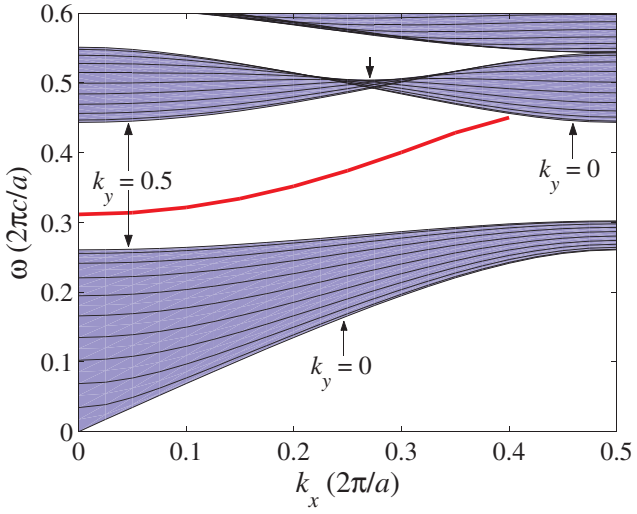

FIG. 2 (color). The projected TM band structure of the bulk crystal is shown by the blue areas and the black lines that represent $\omega(k_x)$ curves at constant k_y values ranging from 0 to $0.5(2\pi/a)$ in steps of $0.05(2\pi/a)$. Note that the second band of bulk crystal has a saddle point singularity that is indicated by a thick black arrow. Also shown is the dispersion relation of the fundamental waveguide mode (red curve).

lowest photonic bands $\omega(k_x, k_y)$ are plotted as a set of $\omega(k_x)$ curves at constant k_y values ranging from 0 to $0.5(2\pi/a)$ in steps of $0.05(2\pi/a)$. We note, in particular, the twisted shape of the second band, including a saddle point Van Hove singularity located at $k_{x,s} = k_{y,s} = 0.269(2\pi/a)$, $\omega_s = 0.504(2\pi c/a)$ and marked in Fig. 2 by a small arrow. Because of the square symmetry of the crystal, the saddle point is oriented with the maximum positive curvature in the ΓM ($k_x = k_y$) direction, and the maximum negative curvature in the perpendicular direction. As a result, the curvature in the x and y directions is very small [also see Fig. 4(d)]. This, together with the requirement of zero group velocity of the bands at the Brillouin zone edge, translates into a very flat band $\omega(k_y)$ at $k_x = k_{x,s}$, the relative width of the band from one Brillouin zone edge to the other being just 2% of the central frequency.

The saddle point singularity leads to a complex structure of the evanescent modes at band-gap frequencies immediately above or below it. For the case of the waveguide mode considered here, it is the region below the saddle point that is relevant for the surprisingly strong confinement. To show this, in Figs. 3(a)–3(d) we plot the complex-valued $k_y^{(n)}$ solutions for the bulk as a function of frequency for four values of the axial wave vector k_x that span the first Brillouin zone range. In each plot, the real and imaginary parts of $k_y^{(n)}$ are plotted side by side. In the frequency range of interest only the two lowest-order solutions (labeled $n = 0$ and $n = -1$ by equivalence to the vacuum modes mentioned above) have relatively small imaginary parts. We can safely ignore higher-order evanescent modes that are much more rapidly decaying and do not contribute to the overall confinement strength κ. For $k_x = 0$ [Fig. 3(a)], we locate a photonic band gap in the frequency range 0.26–0.44 $(2\pi c/a)$. The gap is qualitatively similar to the gap of a one-dimensional photonic crystal: it is relatively symmetric, with the maximum confinement strength near the middle of the gap. Also the gap is bounded below and above (points A and B) by propagating solutions belonging to the same mode ($n = 0$). However, when we move to larger values of k_x we see dramatic changes in the nature of the band gap and in the nature of the photonic band just above the gap. Because of the presence of the saddle point, the slope of the second band changes sign from $k_x = 0$ to $k_x = 0.5$ resulting in an intermediate ultraflat regime as seen for $k_x = 0.3$ [Fig. 3(c)]. In this ultraflat regime, the small curvature of

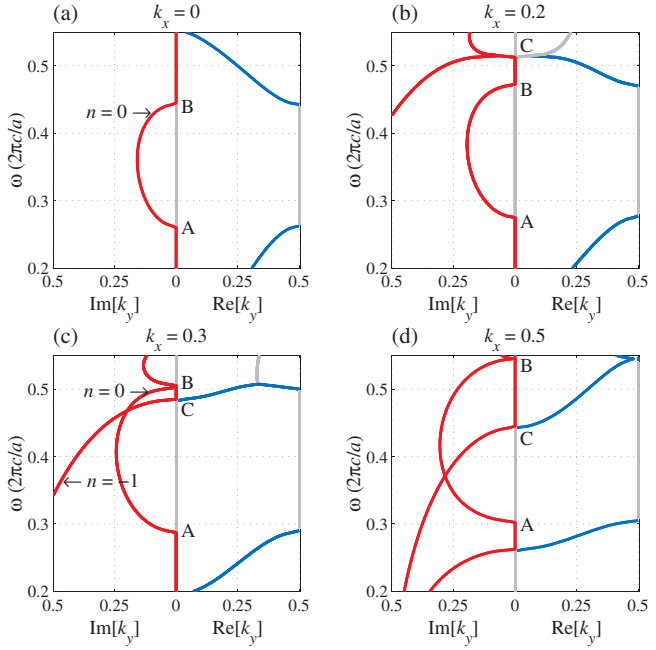

FIG. 3 (color). Dispersion relations $\omega(k_y^{(n)})$ at fixed k_x for propagating and evanescent modes in the bulk crystal. The axial wave vector k_x takes the values 0, 0.2, 0.3, and $0.05(2\pi/a)$ for parts (a) through (d). The imaginary part of $k_y^{(n)}$ is shown in red on the left side of each plot, while the real part is shown on the right, in blue for propagating modes and gray for evanescent and complex modes. In parts (a) and (c), the individual modes $k_y^{(n)}$ are labeled by the value of their n index. The A and B labels track the range of frequencies for which the $n = 0$ mode is evanescent, while the C label tracks the cutoff frequency of the $n = -1$ mode.

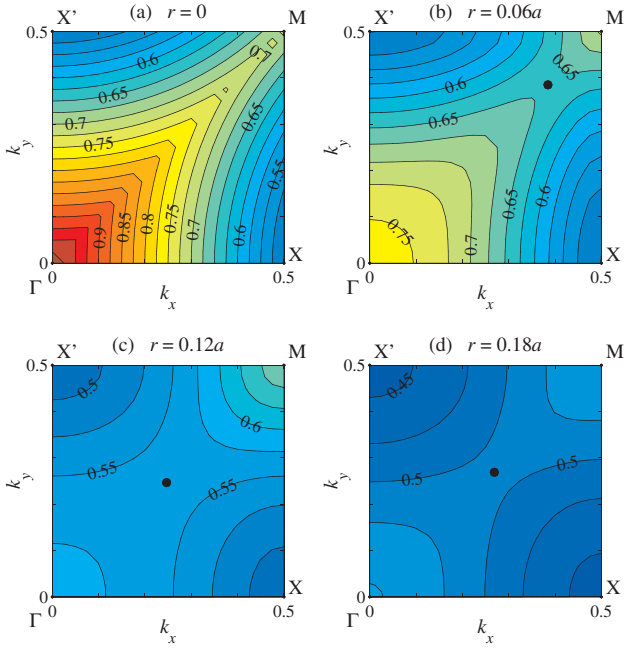

FIG. 4 (color). Contour plots of the second photonic crystal band $\omega(k_x, k_y)$ for varying radii of the dielectric rods: (a) $r = 0$ (vacuum), (b) $r = 0.06a$, (c) $r = 0.12a$, and (d) $r = 0.18a$. The same color scheme is used for all four parts of the figure. Constant-frequency contours are labeled by the corresponding value of the angular frequency ω in units of $(2\pi c/a)$. In parts (b), (c), and (d), a black dot indicates the position of the saddle point Van Hove singularity.

$\omega(\mathrm{Re}[k_y])$ near the cutoff points B and C translates into an equally small curvature for $\omega(\mathrm{Im}[k_y])$ just below the cutoffs. As a result, the confinement map becomes very asymmetric. This can be clearly seen at $k_x = 0.3$, for example, where the confinement strength increases sharply as we move down in frequency from the cutoff at point C. To be more quantitative, we note that in the upper part of the gap the confinement strength reaches $\kappa = 0.20(2\pi/a)$ at a frequency that is only $0.017(2\pi c/a)$ below the gap edge C, while in the lower part of the gap, the same confinement strength is reached at a frequency $0.052(2\pi c/a)$ above the gap edge A. This ratio of almost 3 between the steepness of κ near the upper and lower band edges is also visible in Fig. 1(b) and is the main cause for the strong asymmetry of the localization strength along the waveguide mode dispersion relation [Fig. 1(c)].

The presence of a saddle point in the second photonic band and the associated enhanced confinement is not just an accident for the particular parameters of the bulk photonic crystal considered above. In Figs. 4(a)–4(d) we present color contour plots of the dispersion relation $\omega(k_x, k_y)$ of the second band when the radius r of the dielectric rods is increased from 0 to $0.06a$, $0.12a$, and $0.18a$. For values of $r > 0$ the photonic band always has a saddle point Van Hove singularity [shown as a black dot in Figs. 4(b)–4(d)] in the middle of the band, away from the symmetry points. The interior saddle point clearly leads to ultraflat regions of the photonic bands in Figs. 4(c) and 4(d). We argue that this saddle point must exist for $r > 0$ because (i) all points along the ΓM symmetry line are maxima in the direction perpendicular to ΓM and (ii) $\omega(k, k)$ has a minimum somewhere between Γ and M. Part (i) is due to a mirror symmetry across ΓM and to an anticrossing between the second and third bands. Part (ii) comes from the combination of the normal "kinetic" contribution that makes the frequency increase from M to Γ [as seen from the vacuum band in Fig. 4(a)] and a periodicity-induced repulsion between bands 2 and 4. This repulsion is canceled at the M point because the two bands belong to different irreducible representations, but it becomes strong as we move away from the M point, and thus leads to the minimum point in the $\omega(k, k)$ curve. The repulsion mechanism is similar to the one responsible for anomalous dispersion relations in axially uniform waveguides [14]. From the same topological and perturbative arguments used above it follows that such an interior saddle point will be present in the TM and TE band structures of other square 2D photonic crystals as well. Band structures of three-dimensional (3D) crystals exhibit

two types of saddle point singularities that have the canonical form $\omega - \omega_0 = \pm(\alpha_x k_x^2 + \alpha_y k_y^2 - \alpha_z k_z^2)$ and are topologically different from their two-dimensional counterpart [15]. The strongest extension of the effects presented here to the case of a waveguide in a 3D crystal would be obtained if the saddle point could cause a two-dimensional ultraflat region in the dispersion relation (ω varying slowly with $\mathbf{k}$ in two directions) such that band-gap confinement is enhanced in both lateral directions. This may be difficult to obtain in general and only achievable for special cases of the coefficients $\alpha_{x,y,z}$. Nevertheless, it is still true that saddle points lead to ultraflat bands in certain *directions* of $\mathbf{k}$ space (e.g., the [011] direction for the canonical form above if $\alpha_y = \alpha_z$) and consequently can result in enhanced confinement in those directions for gap frequencies in the vicinity of ω_0, just as in the two-dimensional case.

The results presented here obviously have important consequences for the tunneling of photons through photonic crystals. Even more interestingly, they also extend to the tunneling of electrons through crystalline barriers. Such barriers are found, for example, in magnetic tunnel junctions (MTJs), which have been the focus of recent research due to their large tunneling magnetoresistance [16]. Mavropoulos *et al.* [17] have shown that important conclusions about spin-dependent tunneling in MTJs can be drawn by analyzing the evanescent states inside the gap of the insulator material. We suggest that the presence of a saddle point near the band gap will result in rapidly decaying evanescent states for electron energies in the vicinity of the band edge. This strong variation of the decay parameter κ as a function of energy will result in an increased energy sensitivity of the tunnel current through the barrier and, consequently, an increased tunneling magnetoresistance.

In conclusion, we have shown that the presence of a saddle point in the band structure of a photonic crystal can lead to enhanced band-gap confinement away from midgap. This explains the recently observed anomalous radiation loss of a photonic crystal waveguide mode and suggests that, in general, one can make use of such saddle points to improve the design of other photonic and electronic devices that rely on band-gap confinement.

This work was supported in part by the Materials Research Science and Engineering Center program of the National Science Foundation under Grant No. DMR 02-13282.

*Present address: Lawrence Livermore National Laboratory, Livermore, CA 94550, USA.

[1] E. Yablonovitch, Phys. Rev. Lett. **58**, 2059 (1987).
[2] S. John, Phys. Rev. Lett. **58**, 2486 (1987).
[3] J. D. Joannopoulos, P. R. Villeneuve, and S. Fan, Nature (London) **386**, 143 (1997).
[4] A. Chutinan and S. Noda, Phys. Rev. B **62**, 4488 (2000).
[5] A. Mekis, J. C. Chen, I. Kurland, S. Fan, P. R. Villeneuve, and J. D. Joannopoulos, Phys. Rev. Lett. **77**, 3787 (1996).
[6] M. Bayindir, E. Ozbay, B. Temelkuran, M. M. Sigalas, C. M. Soukoulis, R. Biswas, and K. M. Ho, Phys. Rev. B **63**, 081107 (2001).
[7] Z. Y. Li and K. M. Ho, Phys. Rev. Lett. **92**, 063904 (2004).
[8] N. W. Ashcroft and N. D. Mermin, *Solid State Physics* (Holt Saunders, Philadelphia, 1976).
[9] J. O. Vasseur, L. Dobrzynski, B. DjafariRouhani, and H. Puszkarski, Phys. Rev. B **54**, 1043 (1996).
[10] J. V. Sanchez-Perez, D. Caballero, R. Martinez-Sala, C. Rubio, J. Sanchez-Dehesa, F. Meseguer, J. Llinares, and F. Galvez, Phys. Rev. Lett. **80**, 5325 (1998).
[11] J. Smajic, C. Hafner, K. Rauscher, and D. Erni, in *Progress in Electromagnetics Research Symposium PIERS, Pisa, 2004*, edited by T. E. Academy, Vol. 1, pp. 21–24.
[12] Y.-C. Hsue and T.-J. Yang, Solid State Commun. **129**, 475 (2004).
[13] P. Bienstman and R. Baets, Opt. Quantum Electron. **33**, 327 (2001).
[14] M. Ibanescu, S. G. Johnson, D. Roundy, C. Luo, Y. Fink, and J. D. Joannopoulos, Phys. Rev. Lett. **92**, 063903 (2004).
[15] L. Van Hove, Phys. Rev. **89**, 1189 (1953).
[16] E. Y. Tsymbal, O. N. Mryasov, and P. R. LeClair, J. Phys. Condens. Matter **15**, R109 (2003).
[17] P. Mavropoulos, N. Papabikolaou, and P. H. Dederichs, Phys. Rev. Lett. **85**, 1088 (2000).